Research Square

Preprints are preliminary reports that have not undergone peer review.
They should not be considered conclusive, used to inform clinical practice,
or referenced by the media as validated information.

Boundary-Guided U-Transformer for Automatic Stratigraphic Correlation from Multichannel Well Logs

Jian Yang

273638419@qq.com

Southwest Petroleum University

Xuri Huang

Southwest Petroleum University

Yumao Chen

Shengli Oilfield Company, Sinopec

Jing Tang

Southwest Petroleum University

Yuxiao Zhang

Shengli Oilfield Company, Sinopec

Method Article

Keywords: stratigraphic correlation, Multichannel well logs, Boundary-Guided U-Transformer, Boundary detection, Sequence-constrained Viterbi decoding

Posted Date: November 9th, 2026

DOI: https://doi.org/10.21203/rs.3.rs-11339676/v1

License: This work is licensed under a Creative Commons Attribution 4.0 International License.
Read Full License

Additional Declarations: No competing interests reported.

Boundary-Guided U-Transformer for Automatic Stratigraphic Correlation from Multichannel Well Logs

Jian Yang[1,2] · Xuri Huang[1,2] · Yumao Chen[3] · Jing Tang[1,2] · Yuxiao Zhang[3]

[1] School of Geosciences and Technology, Southwest Petroleum University, Chengdu 610500, China
[2] State Key Laboratory of Oil and Gas Reservoir Geology and Exploitation, Southwest Petroleum University, Chengdu 610500, China
[3] Geophysical Research Institute, Shengli Oilfield Company, Sinopec, Dongying 257022, Shandong, China
*Corresponding author: Jian Yang, e-mail: 273638419@qq.com

Abstract

Fine-scale stratigraphic correlation supports reservoir characterization, but manual interpretation is time-consuming and may vary among interpreters. This study proposes a Boundary-Guided U-Transformer (BG-UT) for automatic stratigraphic correlation from multichannel well logs. The method formulates correlation as a one-dimensional semantic segmentation task along the depth direction. A U-shaped convolutional encoder–decoder with skip connections is combined with a Transformer bottleneck incorporating relative positional bias, enabling the network to integrate local well-log response patterns with information from a broader depth interval. Auxiliary branches for stratigraphic top/base regression and boundary detection are jointly optimized with the classification task, providing complementary supervision for interval geometry and interface positions. During inference, sequence-constrained Viterbi decoding combines classification scores with transition preferences based on the expected vertical succession, encouraging stratigraphically coherent label sequences. The decoded labels are then converted into contiguous stratigraphic intervals and top/base-depth tables. On 60 validation wells, BG-UT achieves an average accuracy of 82.09% and a macro F1-score of 84.89%, exceeding SegNet and Encoder Transformer by 4.46 and 2.71 percentage points in average accuracy, respectively. The proposed method effectively improves boundary localization stability, reduces the influence of local abnormal log responses and stratigraphic thickness variations, and provides a reliable intelligent approach for fine-scale stratigraphic correlation and subsequent reservoir modeling under complex reservoir conditions.

Keywords: stratigraphic correlation · Multichannel well logs · Boundary-Guided U-Transformer ·Boundary detection ·Sequence-constrained Viterbi decoding

Introduction

Fine-scale stratigraphic correlation establishes the correspondence of reservoir units among wells and provides the stratigraphic framework required for reservoir characterization. Reliable correlation is essential for describing sand-body distribution, reservoir heterogeneity, and the spatial organization of remaining oil (Liu et al. 2022; Xu et al. 2025). In mature oilfields, however, dense well coverage and numerous stratigraphic subdivisions make manual correlation time-consuming. Interpretation may also vary among geologists, particularly where log responses are ambiguous or stratigraphic thickness changes between wells. Automatic correlation therefore requires methods that can identify stratigraphic units consistently while retaining the geological meaning of their boundaries.

Early automatic methods established correlation through similarities between well-log curves. Cross-correlation and related shifting or stretching techniques provided computational approaches to matching subsurface sequences (Rudman and Lankston 1973; Mann and Dowell 1978). Dynamic depth warping and dynamic time warping subsequently allowed local variations in stratigraphic thickness, while knowledge-based constraints incorporated additional geological information into the matching process (Lineman et al. 1987; Wheeler and Hale 2014). More recent developments have combined signal transformation, statistical assessment, relative geologic time, and seismic constraints with sequence matching to support multi-well correlation (Behdad 2019; Sylvester 2023; Dai et al. 2025; Lu et al. 2025). These approaches

extend the applicability of automated matching, although their performance remains sensitive to reference information, preprocessing choices, and the constraints used to distinguish similar responses in different stratigraphic intervals.

Deep learning provides an alternative by learning stratigraphic representations directly from multichannel well logs. Encoder–decoder methods formulate stratigraphic subdivision as a segmentation problem and assign class labels to individual depth samples. Multitask encoder–decoder learning has also been applied to sublayer interpretation. Dai et al. (2026) employ a multitask SegNet for automated well stratigraphic interpretation and subsequently extend the approach to seismic-constrained spatial mapping for reservoir property modeling. Liu et al. (2022) propose an edge-guided feature pyramid network that combines multiscale feature extraction with auxiliary boundary supervision. Yang et al. (2023) introduce attention weighting and densely connected convolutions to improve feature representation. Wang et al. (2024) combine label smoothing with spatial and channel attention and apply confidence-based constraints during prediction to reduce repeated stratigraphic assignments. An alternative formulation treats stratigraphic intervals as detection targets, allowing interval identification and boundary localization through an improved YOLOv8 model (Tang et al. 2024). Transformer-based methods further incorporate relationships between well-log responses at different depths. ASHFormer combines high-resolution representations with axial and sliding-window attention to capture local and long-range information (Liu et al. 2023). Xu et al. (2025) integrate convolutional and Transformer representations and introduce geological constraints into the training loss. OMP-KANFormer combines nonlinear feature learning and Transformer encoding with waveform-based data augmentation to support training-dataset construction (Zhang et al. 2025). These developments demonstrate the relevance of multiscale representation, boundary-related supervision, and geological constraints to automatic stratigraphic interpretation.

These developments suggest three complementary requirements for fine-scale stratigraphic correlation. First, local variations in well-log responses must be resolved to distinguish adjacent sublayers and locate their boundaries. Multiscale convolutional feature extraction and high-resolution skip connections address this requirement, while top/base-depth regression and boundary-detection supervision provide additional guidance for interface localization. Second, similar log responses occurring in different stratigraphic units must be distinguished using information from a broader depth interval. Transformer self-attention addresses this requirement by modeling relationships between well-log responses at different depths, with relative positional bias representing their separation along the depth sequence. Third, the predicted labels must form a sequence consistent with the expected stratigraphic succession. This requirement is addressed through a geological transition model and Viterbi decoding, which combine classification scores with stratigraphic-order constraints. These considerations motivate a framework that integrates local feature extraction, long-range sequence modeling, boundary supervision, and sequence-constrained decoding.

Building on these considerations, this study proposes a Boundary-Guided U-Transformer (BG-UT) for automatic stratigraphic correlation from multichannel well logs. The architecture combines a U-shaped convolutional encoder–decoder with a Transformer bottleneck, integrating local log-response features with relationships across the depth sequence. Joint training of stratigraphic classification, top/base-depth regression, and boundary detection provides complementary supervision for sublayer identification and interface localization. During inference, a geological transition model and Viterbi decoding guide the predicted labels toward the expected stratigraphic order, after which contiguous intervals are converted into stratigraphic-top tables. The complete framework is compared with one-dimensional SegNet and Encoder Transformer models using the same well-level training and validation partition. Overall and class-wise metrics assess classification performance, paired comparisons before and after decoding examine the effect of sequence constraints, and applications to unlabeled wells illustrate the construction of well-level subdivisions and multi-well correlation sections.

Methodology

Problem formulation and overall workflow

Automatic stratigraphic correlation is formulated as a supervised sequence-labeling problem in which multichannel well-log responses are mapped to stratigraphic classes along depth. Expert-interpreted stratigraphic interfaces provide additional supervision for learning the positions of interval boundaries. The objective is to identify stratigraphic units at individual depth samples and convert the resulting predictions into continuous intervals consistent with the expected stratigraphic succession. The overall workflow comprises model training and model inference, as illustrated in Fig. 1.

The logging channels are aligned on a common depth grid within a prescribed analysis window. The input sequence is expressed as

$$X_i = [x_i^{(1)}, x_i^{(2)}, \dots, x_i^{(C)}]^T \in R^{C\times L}, \quad (1)$$

where $x_i^{(C)} \in R^L$ contains the measurements of logging channel C, C is the number of input channels, and L is the number of depth samples. For a uniformly sampled sequence, the measured depth of sample ℓ is

$$d_l = d_0 + \ell\Delta d, \qquad \ell = 0,1, \dots, L-1, \quad (2)$$

where d_0 is the first depth in the analysis window and Δd is the sampling interval. The deepest sample is therefore located at $d_{max} = d_0 + (L-1)\Delta d$. The logging channels, sampling interval, analysis window, and target stratigraphic units are specified for the application under consideration.

Expert-interpreted top and base depths are converted into point-wise class labels. Let K_{tar} denote the number of target stratigraphic units. The reference label at sample ℓ in well i is defined as

$$y_{i,\ell} \in \{0,1, \dots, K_{tar}\}, \quad (3)$$

where class 0 represents the background and classes 1,…, K_{tar} identify the target units. Samples outside the interpreted target intervals are assigned to the background class. The total number of classification outputs, including the background, is $K = K_{tar} + 1$. The numerical labels identify stratigraphic classes, while their expected succession is specified separately through the transition model used during inference.

Two additional targets are constructed to provide supervision related to stratigraphic interfaces. For a sample belonging to target unit k, the normalized top/base-depth target is

$$r_{i,l} = \left[\frac{t_{i,k} - d_0}{d_{max} - d_0}, \frac{b_{i,k} - d_0}{d_{max} - d_0}\right], \quad (4)$$

where $t_{i,k}$ and $b_{i,k}$ are the interpreted top and base depths of unit k in well i. This normalization expresses the interface positions relative to the analysis window. A validity mask $v_{i,\ell}$ is assigned a value of 1 where valid interpreted top and base depths are available and 0 otherwise, so that the regression loss is evaluated only for samples with defined boundary targets.

A binary boundary-detection target is generated from changes in the reference class sequence:

$$e_{i,\ell} = \begin{cases} 0, \ell = 0, \\ 1, \ell \geq 1 \; and \; y_{i,\ell} \neq y_{i,\ell-1}, \\ 0, \ell \geq 1 and \; y_{i,\ell} = y_{i,\ell-1}, \end{cases} \quad (5)$$

Thus, $e_{i,\ell}$ marks a transition between adjacent class labels. Together, the classification, top/base-regression, and boundary-detection targets supervise stratigraphic identity, interval geometry, and local interface transitions, respectively.

During model training, the Boundary-Guided U-Transformer (BG-UT) learns these three tasks from labeled well-log sequences through a shared feature representation. The classification task supervises the identification of stratigraphic units, while the two auxiliary tasks introduce information about interface positions and adjacent-label transitions. The network architecture and joint learning objective are detailed in the subsections "Boundary-guided U-Transformer architecture" and "Multi-task learning objective," respectively.

During model inference, a well-log sequence is passed through the trained BG-UT to obtain point-wise classification scores. These scores are combined with a transition model representing the expected stratigraphic succession. Viterbi decoding determines the label sequence that maximizes the combined emission and transition scores, thereby incorporating stratigraphic-order preferences into the interpretation of the network predictions. The decoded sequence is subsequently refined and grouped into contiguous intervals, from which top and base depths are extracted to construct a stratigraphic-top table. The decoding and interval-extraction procedures are detailed in the subsection "Sequence-constrained decoding and stratigraphic-top extraction."

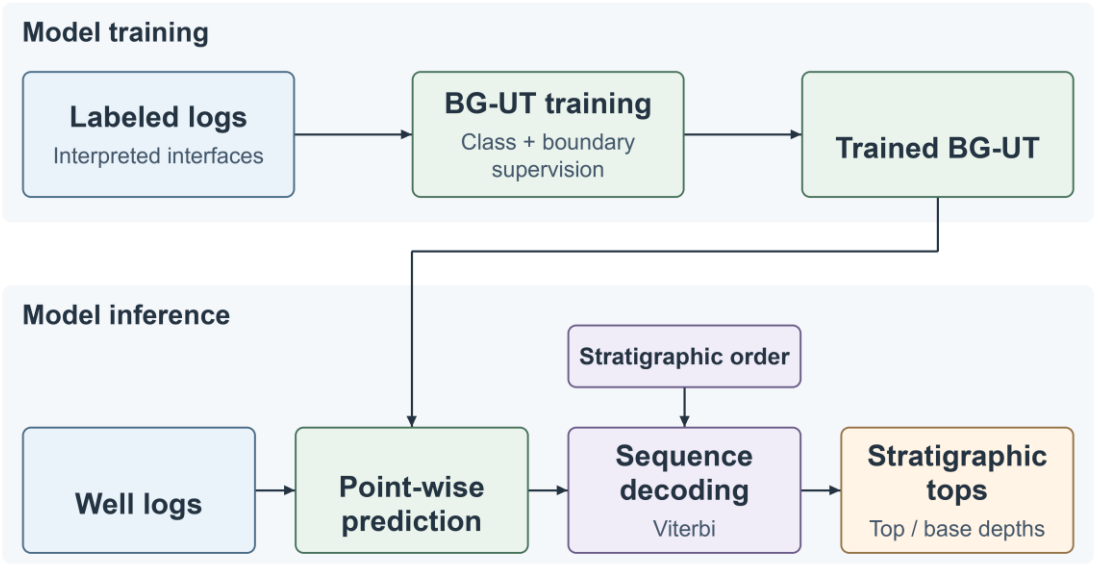


Fig. 1 A workflow of automatic stratigraphic correlation.

Comparative network architectures

A one-dimensional SegNet and an Encoder Transformer are considered as reference architectures for automatic stratigraphic correlation. Both models process multichannel well-log sequences and produce point-wise stratigraphic classifications together with normalized top/base-depth predictions. Their architectures provide two approaches to combining feature extraction and depth-resolution reconstruction: convolutional encoding–decoding with pooling-index recovery, and convolutional feature extraction combined with self-attention.

The one-dimensional SegNet adapts the pooling-index-based encoder–decoder design of Badrinarayanan et al. (2017) to multichannel well-log sequences (Fig. 2). The encoder applies successive convolutional stages with batch normalization and rectified linear unit activation to extract well-log response patterns at progressively coarser resolutions. Max-pooling reduces the sequence length and enlarges the receptive field, while the positions selected by each pooling operation are retained as pooling indices. The decoder uses the corresponding indices during max-unpooling to place the features at their recorded positions, followed by convolutional transformation to reconstruct the feature sequence. The recovered features are passed to a classification head and a top/base-regression head, which predict stratigraphic class scores and normalized interface positions at individual depth samples.

The Encoder Transformer combines multiscale convolutional feature extraction with attention-based sequence modeling (Fig. 3). Parallel one-dimensional convolutions with different kernel sizes extract response patterns over different depth intervals. Their outputs are concatenated and projected into a shared feature space. A strided convolution then reduces the sequence length before Transformer encoding, allowing self-attention to operate on a compressed representation with lower computational cost.

The Transformer encoder follows the self-attention framework introduced by Vaswani et al. (2017), in which multi-head attention enables each feature vector to incorporate information from other positions in the compressed depth sequence. Feed-forward transformations, residual connections, layer normalization, and dropout are used within the encoder blocks. A learnable relative positional bias accounts for the separation between sequence positions when calculating attention scores. The encoded features are subsequently interpolated to the original depth resolution and fused with the local convolutional features. As in SegNet, the fused representation supports point-wise classification and normalized top/base-depth regression.

These architectures provide complementary reference approaches. SegNet reconstructs the depth resolution through pooling-index-based decoding, whereas the Encoder Transformer combines local convolutional

features with relationships represented across the compressed sequence. Building on these architectural considerations, BG-UT places a Transformer bottleneck within a U-shaped convolutional encoder–decoder. Corresponding encoder and decoder stages are linked through skip connections, and the shared decoder features support an additional boundary-detection task. This design combines hierarchical feature reconstruction, information from a broader depth interval, and interface-related supervision within the proposed network.

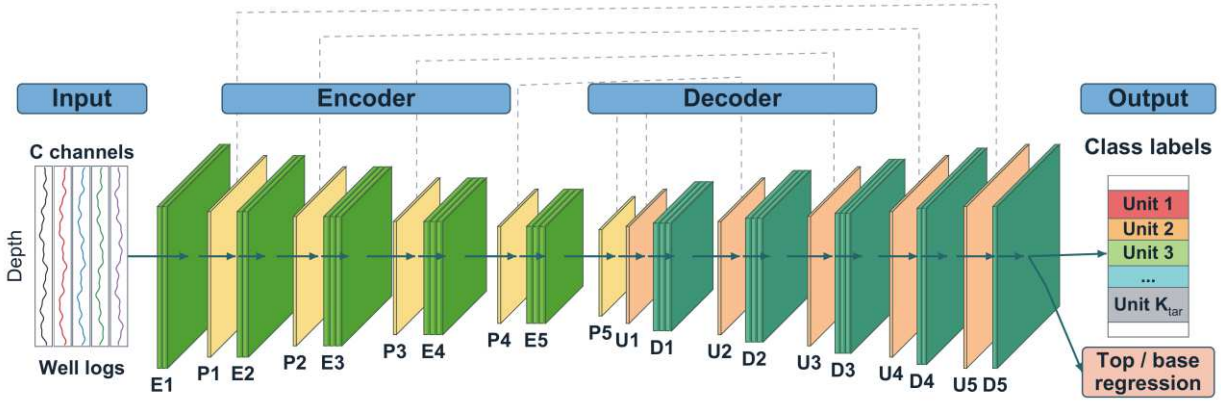


Fig. 2 Architecture of the one-dimensional SegNet model for automatic stratigraphic correlation.

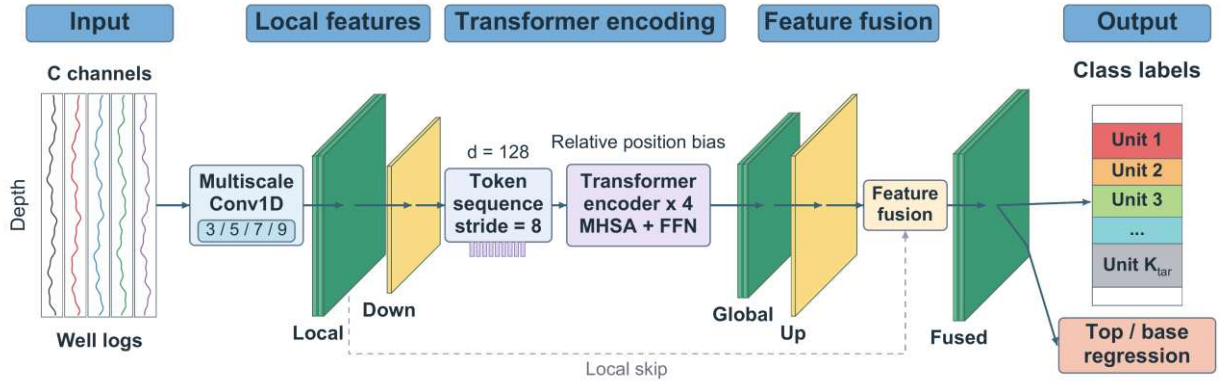


Fig. 3 Architecture of the Encoder Transformer model for automatic stratigraphic correlation.

Boundary-guided U-Transformer architecture

The Boundary-Guided U-Transformer (BG-UT) comprises a one-dimensional convolutional encoder, a Transformer bottleneck, a convolutional decoder with skip connections, and three task-specific prediction heads (Fig. 4). Its convolutional encoder–decoder follows the U-shaped design of Ronneberger et al. (2015), with skip connections transferring features between corresponding encoder and decoder stages. The convolutional pathway extracts local well-log response patterns, while the Transformer represents relationships between responses at different depths within the analysis window. The decoder combines these representations with features retained at finer resolutions. Joint supervision of stratigraphic classification, top/base-depth regression, and boundary detection introduces information about both stratigraphic identity and interface position into the shared features.

The encoder processes the input sequence through successive double-convolution blocks, each comprising one-dimensional convolutions, batch normalization, and rectified linear unit activation. Downsampling

progressively reduces the sequence length and enlarges the receptive field. Features at shallower stages retain fine-scale variations in the logging responses, whereas deeper features represent patterns over broader depth intervals. The outputs of the encoder stages are retained for subsequent transfer to the corresponding decoder stages.

At the bottleneck, the compressed convolutional features are projected into a sequence of feature vectors and processed by Transformer encoder blocks. Multi-head self-attention follows the formulation of Vaswani et al. (2017), allowing a feature vector at one depth position to incorporate information from other positions in the compressed sequence. This mechanism is useful when similar local responses occur in different stratigraphic units and their interpretation requires information from the surrounding depth interval. For an individual attention head, the operation is expressed as

$$Attention(Q,K,V) = softmax\left(\frac{QK^T}{\sqrt{d_h}} + B\right)V, \quad (6)$$

where, Q, K, and V are the query, key, and value matrices, respectively; d_h is the key-vector dimension of the attention head; and B is the learnable relative positional bias. Following the general additive relative-position-bias formulation described by Raffel et al. (2020), the learnable bias B is added to the attention scores to represent the separation between positions along the depth sequence. Attention therefore accounts for both feature similarity and relative depth position. The outputs of the attention heads are combined and further transformed by the feed-forward layers. Attention is applied at the compressed resolution to reduce the computational cost of modeling relationships across the analysis window.

The decoder progressively restores the feature sequence to the original sampling resolution through linear upsampling and convolutional transformation. At each corresponding resolution, the upsampled decoder features are concatenated with features transferred from the encoder through skip connections. This fusion provides access to finer variations retained at earlier encoding stages while incorporating information from the broader depth interval represented at the bottleneck. The final decoder representation supports predictions at individual depth samples.

Three prediction heads operate on the shared decoder features. The classification head produces scores for the target stratigraphic classes and the background class. The top/base-regression head produces two continuous outputs representing the normalized top and base positions of the corresponding stratigraphic interval. The boundary-detection head produces a binary boundary logit indicating a transition between adjacent class labels. The reference targets for these tasks are defined in the problem formulation.

During training, gradients from the three tasks update the shared encoder, Transformer bottleneck, and decoder. The regression task introduces supervision related to interval geometry, while the detection task supervises local class transitions. Together with classification, these auxiliary objectives guide the shared representation toward features relevant to stratigraphic identification and interface localization. The joint learning objective is presented in the following subsection.

During inference, the classification scores are processed by the sequence-constrained decoding procedure detailed below. The auxiliary regression and detection branches provide supervision during training; their predictions are not directly included in the Viterbi decoding objective. BG-UT therefore combines local feature extraction and information from a broader depth interval with boundary-related supervision, while the subsequent decoding stage incorporates the prescribed stratigraphic-order preferences.

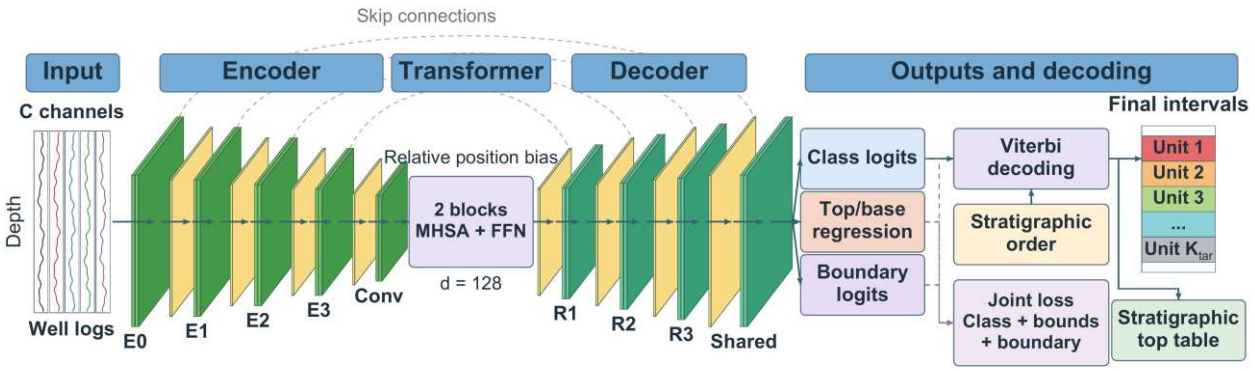


Fig. 4 Architecture of the proposed Boundary-Guided U-Transformer and sequence-constrained decoding strategy.

Multi-task learning objective

BG-UT is trained using a joint objective comprising stratigraphic classification, top/base-depth regression, and boundary detection. Following the shared-representation principle of multitask learning (Caruana 1997), these tasks jointly update the shared encoder, Transformer bottleneck, and decoder. Classification supervises stratigraphic identity at individual depth samples, whereas the auxiliary regression and detection tasks provide complementary supervision for interval geometry and local interface positions. The reference targets are defined in the problem formulation.

For well i, let $z_{i,\ell,k}$ denote the classification logit for class k at depth sample ℓ. The corresponding class probability is

$$p_{i,\ell,k} = \frac{exp(z_{i,\ell,k})}{\sum_{j=0}^{K_{tar}} exp(z_{i,\ell,j})}, k = 0, \dots, K_{tar}, \quad (7)$$

where class 0 represents the background and K_{tar} is the number of target stratigraphic units. Let S denote the set of depth samples in a training mini-batch and $S_{cls} \subseteq S$ the subset with valid classification labels. A weighted cross-entropy objective is used to control the relative contributions of the stratigraphic classes:

$$\mathcal{L}_{cls} = -\frac{\sum_{(i,\ell)\in S_{cls}} w_{y_{i,\ell}} log\ p_{i,\ell,y_{i,\ell}}}{\sum_{(i,\ell)\in S_{cls}} w_{y_{i,\ell}}}, \quad (8)$$

where $y_{i,\ell}$ is the reference class label and $w_{y_{i,\ell}} > 0$ is its assigned weight. A reduced background weight limits its contribution to optimization, while increased weights can emphasize target units that require additional attention during training. The class weights adopted for the field application are specified with the experimental settings.

The regression branch predicts a two-component vector,

$$\hat{r}_{i,\ell} = \left(\hat{r}_{i,\ell}^{top}, \hat{r}_{i,\ell}^{base}\right), \quad (9)$$

representing the normalized top and base depths of the corresponding stratigraphic interval. Given the reference vector $r_{i,\ell}$ and the validity mask $v_{i,\ell}$ defined in the problem formulation, the regression objective is

$$\mathcal{L}_{bnd} = \frac{\sum_{(i,\ell)\in S} v_{i,\ell} \left\| \hat{r}_{i,\ell} - r_{i,\ell} \right\|_1}{2 \sum_{(i,\ell)\in S} v_{i,\ell} + \epsilon}, \quad (10)$$

where ϵ is a small positive constant that prevents division by zero. The factor of two accounts for the top and base components. This objective evaluates the mean absolute error over valid interface targets, providing supervision related to the vertical extent of the stratigraphic interval associated with each sample.

The boundary-detection branch supplies more localized supervision by identifying transitions between adjacent class labels. Let $u_{i,\ell}$ denote its predicted logit and $e_{i,\ell} \in \{0,1\}$ the reference boundary indicator. The predicted boundary probability is $q_{i,\ell} = \sigma(u_{i,\ell})$, where $\sigma(\cdot)$ is the sigmoid function. The binary cross-entropy objective is

$$\mathcal{L}_{edge} = -\frac{1}{|S|} \sum_{(i,\ell)\in S} \begin{bmatrix} e_{i,\ell} log q_{i,\ell} \\ +(1 - e_{i,\ell}) \log(1 - q_{i,\ell}) \end{bmatrix}. \quad (11)$$

Whereas top/base-depth regression associates a sample with the geometry of its stratigraphic interval, boundary detection emphasizes the positions at which neighboring labels change. The two auxiliary tasks therefore provide different forms of interface-related supervision. The complete learning objective is

$$\mathcal{L} = \lambda_{cls}\mathcal{L}_{cls} + \lambda_{bnd}\mathcal{L}_{bnd} + \lambda_{edge}\mathcal{L}_{edge}, \quad (12)$$

where the non-negative coefficients λ_{cls}, λ_{bnd} and λ_{edge} determine the relative contributions of the three tasks. Gradients from the combined objective update the shared representation and the corresponding prediction heads. This joint optimization encourages the learned features to retain information relevant to stratigraphic identity, interval geometry, and local interface transitions. During inference, sequence decoding uses the classification scores; the auxiliary regression and boundary-detection outputs are not directly included in the decoding objective.

Sequence-constrained decoding and stratigraphic-top extraction

Point-wise classification assigns a stratigraphic label independently at each depth sample. Although this approach retains local variations in the network predictions, ambiguous responses near interfaces may produce isolated fragments, repeated intervals, or transitions inconsistent with the expected stratigraphic succession. Sequence-constrained decoding incorporates vertical-order information by evaluating the predicted labels jointly over the analysis window. The decoding procedure and transition-scoring principle are illustrated in Fig. 5.

For a given well, the well index is omitted for clarity. The predicted class probabilities are converted into log-emission scores,

$$E_{\ell,k} = logp_{\ell,k}, \ell = 0, \dots, L-1, \quad (13)$$

where $E_{\ell,k}$ expresses the support provided by the network for assigning class k to sample ℓ. The expected succession of target units is specified as an ordered list of class identifiers,

$$\mathcal{O} = \left(o_1, o_2, \dots, o_{K_{tar}}\right), \quad (14)$$

arranged from shallower to deeper stratigraphic position. This ordering is defined separately from the numerical values used to identify the classes.

A transition-score matrix G describes the relative preference for moving from one class to another between adjacent depth samples. Self-transitions favor continuity within a stratigraphic unit, while forward transitions follow the prescribed succession. Reverse transitions and forward jumps beyond the configured allowance receive strong penalties. Transitions between the background and target classes are retained with separate penalties to reduce scattered background predictions within the target succession. The scores are converted into a row-normalized log-transition matrix,

$$A_{a,b} = G_{a,b} - \log\left(\sum_{c=0}^{K_{tar}} \exp\left(G_{a,c}\right)\right), \quad (15)$$

where $A_{a,b}$ is the log-transition probability from class a to class b. The transition preferences and penalties determine the strength of the stratigraphic prior relative to the classification evidence. The decoded sequence is obtained by maximizing the combined emission and transition scores:

$$\hat{y} = \underset{y\in\{0,\dots,K_{tar}\}^L}{argmax}\left[\sum_{\ell=0}^{L-1} E_{\ell,y_\ell} + \sum_{\ell=1}^{L-1} A_{y_{\ell-1},y_\ell}\right], \quad (16)$$

This optimization is solved using the Viterbi algorithm (Viterbi 1967), which combines dynamic programming with backtracking to recover the highest-scoring label sequence. It identifies the highest-scoring sequence over the complete analysis window, allowing uncertain local predictions to be assessed in relation to neighboring samples and the expected stratigraphic succession. Because the unfavorable transitions receive finite penalties, the formulation imposes soft order constraints rather than strictly excluding every departure from the prescribed succession.

Following decoding, a minimum-thickness filter reduces short predicted fragments. A specified thickness threshold h_{min} is converted into a minimum sample count using the depth increment Δd. Intervals containing fewer than this number of samples are merged into neighboring intervals. For interior fragments, non-background neighbors are preferred where available, and the longer neighboring interval is selected when both are eligible. At the ends of the sequence, the available neighboring interval is used. The operation is repeated until no further eligible short intervals remain. The threshold is an application-specific resolution setting and should be selected with regard to the sampling interval and the thickness of the units to be resolved.

The refined sequence is subsequently grouped into contiguous runs of identical labels, and background runs are excluded from the exported stratigraphic interpretation. For each target interval, the top depth is

assigned to its first sample. Where a subsequent interval exists, the base depth is assigned to the first sample of that interval, so that neighboring intervals share a common interface depth. The terminal interval is closed at the depth limit used for the analysis window. The resulting stratigraphic-top table records the well identifier, stratigraphic-unit name, and predicted top and base depths for each interval.

The extracted interfaces are therefore determined from transitions in the refined classification sequence. The auxiliary top/base-regression outputs contribute through their supervision of the shared network during training, while the transition model introduces stratigraphic-order preferences during inference. Together, these stages convert the learned point-wise classifications into interval-based outputs suitable for subsequent stratigraphic correlation and interpretation.

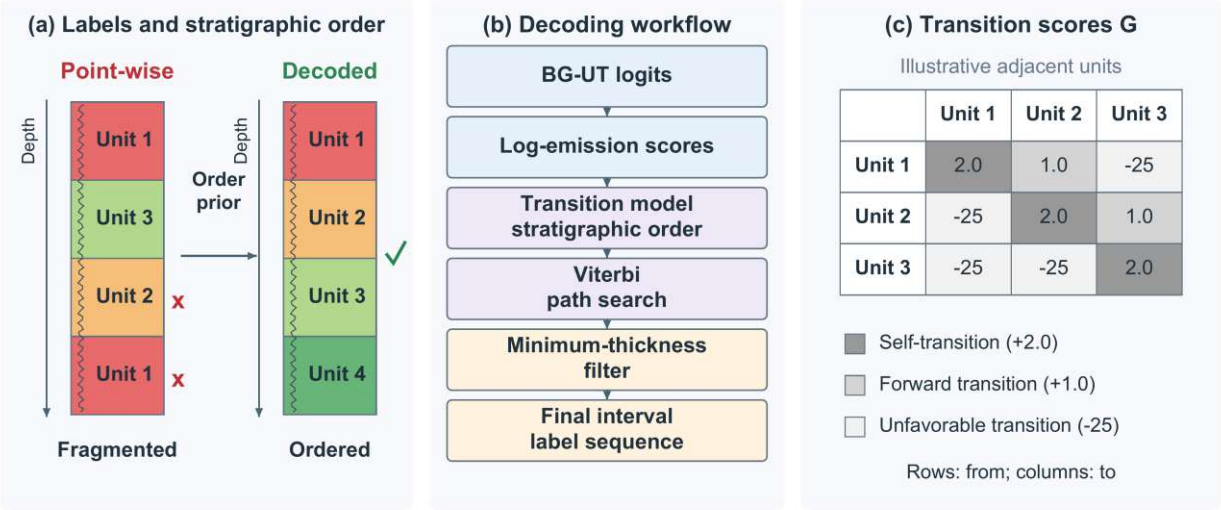


Fig. 5 Principle of sequence-constrained decoding based on geological order and Viterbi search. (a) Direct point-wise prediction may produce reversed or fragmented sublayer labels. (b) Workflow of sequence-constrained decoding from BG-UT logits to the final sublayer label sequence. (c) Example of the geological transition matrix used to encourage self-transitions and forward transitions while penalizing reverse transitions.

Field application and results

Study area and dataset

The study area is located in the central part of a secondary structural belt within a continental rift basin. The reservoir occupies the gently dipping flank of a fault-controlled anticline and is characterized by limited internal faulting, a relatively simple structural configuration, and some edge-water support. The study area covers approximately 23 km², with an average well spacing of less than 125 m. The dense well distribution provides a basis for detailed stratigraphic correlation, sand-body characterization, and sedimentary microfacies analysis (Fig. 6).

The target interval lies within an oil-bearing formation at depths of approximately 1830–2500 m. Deposition occurred in a fluvial–deltaic system, principally within the transition from the delta plain to the delta front. Distributary-channel sand bodies constitute the main reservoir framework, accompanied by mouth-bar, sheet-sand, and mudstone facies. Based on cyclic lake-level fluctuations and sedimentary microfacies associations, the target sand group is subdivided into six sublayers, designated 74, 75, 76, 77, 78, and 79 from shallow to deep. Figure 6 illustrates the subdivision of WELL A1 using the AC, SPCC, COND, ML1, and ML2 logs together with interpreted sublayer boundaries, showing the vertical arrangement of the six sublayers.

The lower and middle sublayers, comprising sublayers 79–75, are dominated by mouth-bar and distributary-channel deposits, together with sheet sands reworked by

lacustrine wave action. In the uppermost sublayer 74, lacustrine regression following a transgressive phase favored the development of delta-plain and delta-front deposits, including mouth bars and distributary channels. Local amalgamation produced composite sand-body belts with relatively good connectivity. The succession shows an upward transition toward delta-plain conditions, with localized swamp development. Overall, the distribution and geometry of the sand bodies reflect the combined influence of lake-level fluctuations and sediment supply. These include isolated channel belts, laterally amalgamated sand bodies, and remnant distributary-channel deposits within sheet sands reworked by lake waves.

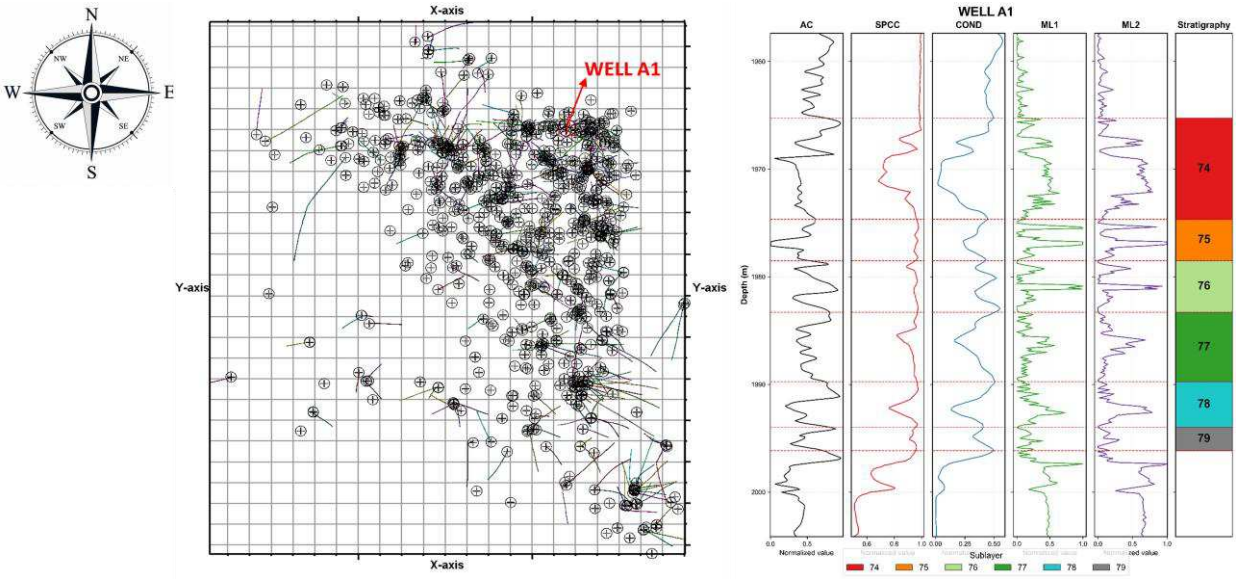


Fig. 6 Well-pattern distribution of the target area and stratigraphic subdivision example of the representative well WELL A1.

Following data matching and quality control, well-log data from 666 wells were retained for this study. Of these, 300 wells had expert-interpreted stratigraphic tops and were used as labeled samples for supervised model development. The remaining 366 wells lacked interpreted tops and were used for automatic stratigraphic subdivision. Five normalized logging curves—AC, ML1, ML2, SPCC, and COND—were used as model inputs. Their complementary responses to lithology, reservoir properties, and fluid conditions provide information for distinguishing the target sublayers.

The original well logs have different sampling intervals, including 0.1 and 0.125 m. To ensure consistent depth sampling across wells and alignment among logging channels, all five channels are resampled onto a common depth grid at an interval of 0.125 m within a fixed analysis window of 1800.0–2299.875 m, yielding 4000 depth samples per well.

For labeled wells, interpreted sublayer tops and bases are mapped onto this grid to generate point-wise stratigraphic labels. Samples outside the interpreted target intervals are assigned to the background class. Evaluation of stratigraphic classification is restricted to samples whose reference labels belong to the six target sublayers.

The 300 labeled wells were divided into 240 training wells and 60 validation wells, with the latter used for model selection and performance evaluation. The trained model was subsequently applied to the 366 unlabeled wells to predict stratigraphic intervals from the multichannel well logs. Table 1 summarizes the dataset and the automatic-correlation task.

Table 1 Summary of the dataset and automatic-correlation task.

Data item	Value
Total retained wells	666 wells
Labeled wells	300 wells
Training wells	240 wells

Validation wells	60 wells	Depth window	1800.0-2299.875 m
Unlabeled wells	366 wells	Sampling interval	0.125 m
Input curves	AC, ML1, ML2, SPCC, COND	Sequence length	4000 points
Target sublayers	74, 75, 76, 77, 78, 79		

Experimental configuration and comparative models

Two comparative models, a one-dimensional SegNet and an Encoder Transformer, are used to evaluate the proposed BG-UT framework. SegNet provides a convolutional encoder–decoder baseline for point-wise stratigraphic classification, whereas Encoder Transformer combines local convolutional features with attention-based representations of relationships over broader depth intervals. Both comparative models include classification and top/base-regression branches. Their architectures are detailed in the subsection "Comparative network architectures" and illustrated in Figs. 2 and 3, respectively. BG-UT additionally incorporates boundary-detection supervision and sequence-constrained decoding. The comparison therefore assesses the performance of the complete prediction frameworks.

The dataset is partitioned at the well level. The 300 labeled wells are divided into 240 training wells and 60 validation wells, corresponding to an 80/20 split. All depth samples from a given well belong to the same subset, so no well contributes samples to both training and validation. The remaining 366 wells are used for automatic correlation without interpreted stratigraphic labels. Figure 7 shows the spatial distribution of the three subsets, together with projected wellbore trajectories.

All three models use the same five input curves, depth sampling interval, analysis window, and well-level partition. Network parameters are optimized using Adam with an initial learning rate of 0.001, a weight decay of 0.0001, and a maximum of 100 training epochs. For BG-UT, the batch size is four, and a cosine-annealing scheduler reduces the learning rate to a minimum of 0.00001. For BG-UT, the classification, top/base-regression, and boundary-detection loss weights are set to 1.0, 0.5, and 1.0, respectively. The class weights used in the classification loss are 0.2 for the background class, 1.5 for sublayers 74 and 75, and 1.0 for the remaining target sublayers. Early stopping is applied when validation accuracy over the target sublayers does not improve for 15 consecutive epochs. The checkpoint with the highest validation accuracy is selected for subsequent inference and evaluation. The random seed is fixed at 42 for data partitioning and model initialization.

During inference, each well-log sequence is passed through the selected model to obtain point-wise class scores and auxiliary top/base predictions. SegNet and Encoder Transformer assign the class with the highest predicted probability to each depth sample. For BG-UT, the classification scores are processed using the sequence-constrained decoding procedure described in the Methodology. The prescribed stratigraphic order is $74 \rightarrow 75 \rightarrow 76 \rightarrow 77 \rightarrow 78 \rightarrow 79$, from shallow to deep. The transition scores include a self-transition bonus of 2.0 and an adjacent forward-transition bonus of 1.0, with penalties of 25.0 for reverse or nonadjacent transitions and 1.5 for transitions between background and target classes. A minimum-thickness threshold of 0.2 m is used to reduce short predicted fragments. The refined labels are grouped into contiguous intervals and exported as stratigraphic-top tables.

Model performance is evaluated against the expert-interpreted labels of the 60 validation wells. Only samples whose reference labels belong to the six target sublayers are included in the main classification evaluation. Predictions of background at these samples remain classification errors. Let Ω_i denote the set of evaluated depth samples in validation well i, and let $y_{i,\ell}$ and $\hat{y}_{i,\ell}$ denote the reference and predicted labels at sample ℓ, respectively. The classification accuracy of well i is

$$Acc_i = \frac{1}{|\Omega_i|} \sum_{\ell \in \Omega_i} I\left(\hat{y}_{i,\ell} = y_{i,\ell}\right), \tag{17}$$

where $I(\cdot)$ equals one when the prediction matches the reference label and zero otherwise. Average accuracy is calculated across the validation wells as

$$Acc_{avg} = \frac{1}{N_{val}} \sum_{i=1}^{N_{val}} Acc_i \,, \tag{18}$$

where $N_{val} = 60$. For each target sublayer k, precision, recall, and F1-score are calculated from the evaluated samples pooled across all validation wells:

$$P_k = \frac{TP_k}{TP_k + FP_k}, \tag{19}$$

$$R_k = \frac{TP_k}{TP_k + FN_k}, \tag{20}$$

$$F1_k = \frac{2P_k R_k}{P_k + R_k}, \tag{21}$$

where TP_k, FP_k, and FN_k represent the true positives, false positives, and false negatives of sublayer k, respectively. To assign equal importance to each target sublayer, macro-averaged metrics are calculated as

$$P_{macro} = \frac{1}{K_{tar}} \sum_{k=1}^{K_{tar}} P_k \,, \tag{22}$$

$$R_{macro} = \frac{1}{K_{tar}} \sum_{k=1}^{K_{tar}} R_k \,, \tag{23}$$

$$F1_{macro} = \frac{1}{K_{tar}} \sum_{k=1}^{K_{tar}} F1_k \,, \tag{24}$$

where $K_{tar} = 6$. Metrics with a zero denominator are assigned a value of zero, and the reported accuracy, precision, recall, and F1-scores are expressed as percentages. Confusion matrices and class-wise F1-scores are used to examine recognition differences among the target sublayers. Representative well plots provide additional comparisons of predicted interval continuity and stratigraphic order. The effect of sequence-constrained decoding is examined separately by comparing BG-UT predictions before and after decoding on the same labeled wells. This paired analysis includes training and validation wells and is distinguished from the validation-only model comparison. Predictions for the 366 unlabeled wells are presented as well-scale interpretations and correlation sections to illustrate the application of the framework.

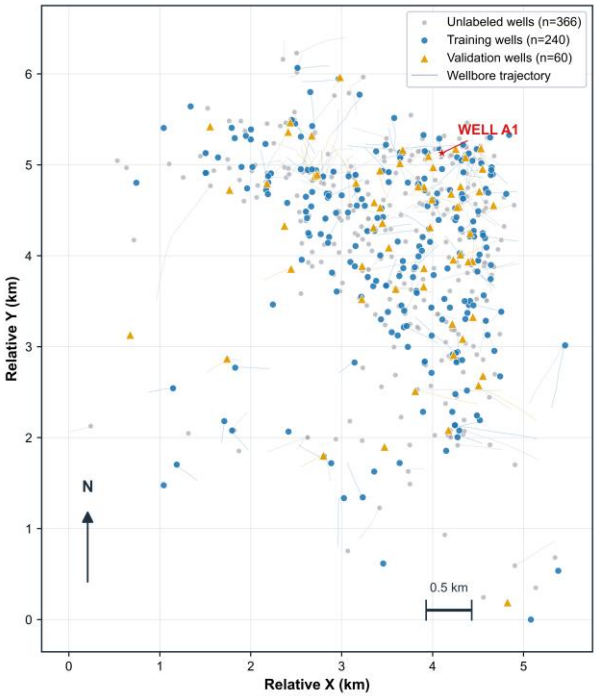


Fig. 7 Spatial distribution of training, validation, and unlabeled wells. Projected wellbore trajectories are shown as faint lines, and different symbols indicate training wells, validation wells, and unlabeled wells.

Training behavior and classification performance

The training behavior of BG-UT is examined using the total loss, individual loss components, and classification accuracy over the target sublayers (Fig. 8). The training loss decreases rapidly during the initial epochs and then declines more gradually, whereas the validation loss decreases initially but exhibits fluctuations during subsequent optimization (Fig. 8a). The classification loss contributes most strongly to the initial training objective and decreases substantially as training progresses. The boundary-regression loss decreases more gradually, while the boundary-detection loss rapidly reaches a low value (Fig. 8b). These curves describe the optimization behavior of the three tasks, although their different magnitudes do not directly indicate their relative prediction performance. Training accuracy rises above 90% in the later epochs, while validation accuracy generally fluctuates between approximately 80% and 90%, with occasional declines (Fig. 8c). The

checkpoint with the highest validation accuracy over the target sublayers is selected for subsequent inference and evaluation.

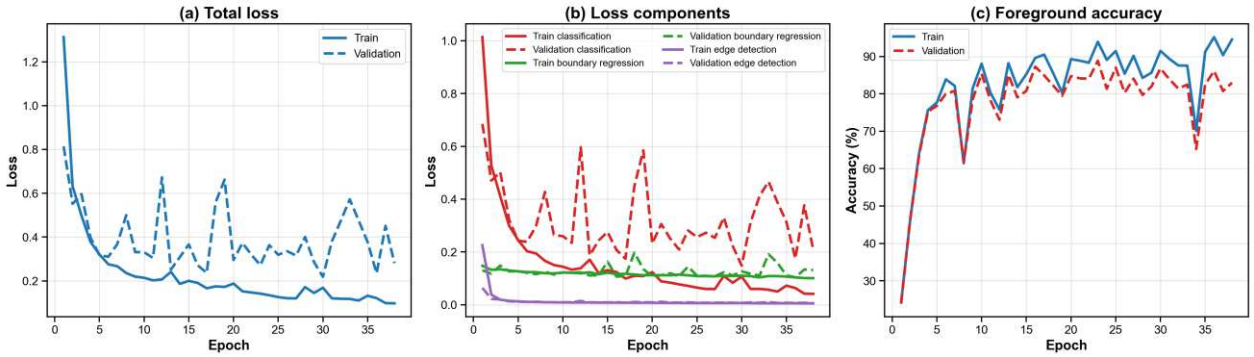


Fig. 8 Training behavior of the proposed BG-UT model. (a) Training and validation total loss curves; (b) classification, boundary-regression, and edge-detection loss components; (c) training and validation target-interval accuracy curves.

Table 2 compares the three models on the 60 validation wells using the evaluation procedure specified in the preceding subsection. BG-UT achieves the highest average accuracy of 82.09%, together with a macro precision of 90.18%, macro recall of 80.35%, and macro F1-score of 84.89%. Its average accuracy exceeds that of SegNet and Encoder Transformer by 4.46 and 2.71 percentage points, respectively. Although Encoder Transformer achieves a higher average accuracy than SegNet, its macro F1-score is lower, at 80.11% compared with 82.25%. This difference indicates that higher average accuracy does not necessarily imply a higher macro-averaged F1-score. BG-UT achieves the highest average accuracy, macro-averaged precision, macro-averaged recall, and macro-averaged F1-score among the three models.

Table 2 Overall performance comparison of SegNet, Encoder Transformer, and BG-UT on the validation wells (n = 60).

Model	Average accuracy (%)	Macro precision (%)	Macro recall (%)	Macro F1-score (%)
SegNet	77.63	89.50	76.45	82.25
Encoder Transformer	79.38	84.60	76.19	80.11
BG-UT	82.09	90.18	80.35	84.89

Beyond the aggregate metrics, a class-wise analysis is essential because overall scores can hide misclassification patterns concentrated near specific sublayers or layer boundaries. Fig. 9 shows that all three models exhibit a clear diagonal dominance in their confusion matrices, confirming that the six target sublayers are broadly distinguishable from multichannel well logs. However, SegNet and Encoder Transformer both show more pronounced off-diagonal responses between adjacent classes, especially around the transitional sublayers. In contrast, the BG-UT confusion matrix shows a more pronounced concentration along the diagonal and fewer misclassifications between several adjacent sublayers. These results support the classification performance of the complete BG-UT framework. The most difficult interval for all three models is 75, which likely reflects its comparatively weak log contrast and transitional depositional characteristics.

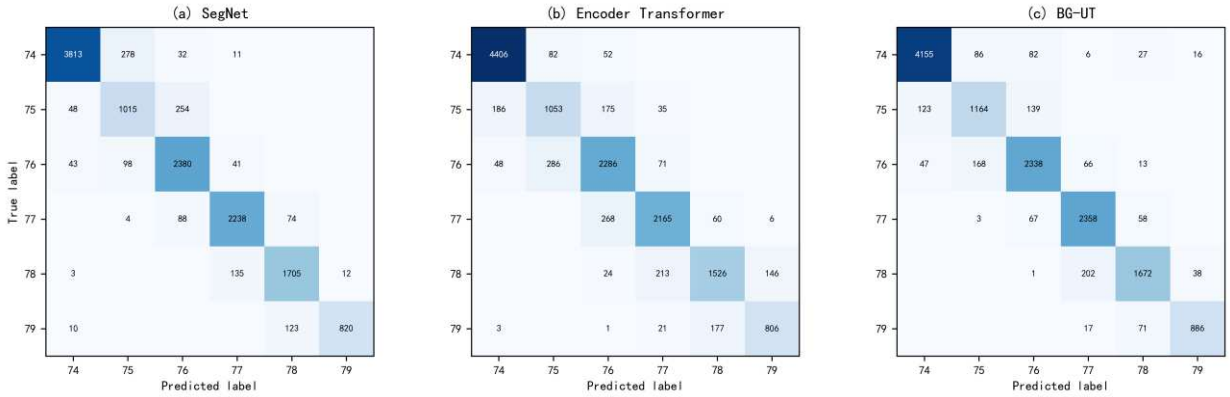


Fig. 9 Confusion matrices of SegNet, Encoder Transformer, and BG-UT on the 60 validation wells, excluding the background class.

The class-wise F1-scores in Fig. 10 further illustrate these differences. BG-UT achieves the highest F1-score for four of the six target sublayers. For sublayer 75, BG-UT attains an F1-score of 77.7%, compared with 68.4% for SegNet and 70.3% for Encoder Transformer. Similar gains are observed for 77 and 79, where BG-UT yields the most balanced recognition across the full target succession. Encoder Transformer performs competitively on 74, but its performance decreases more sharply for the transitional intervals, whereas SegNet tends to produce more errors near layer boundaries and more short, discontinuous predicted intervals. Taken together, the confusion matrices and class-wise F1-scores indicate that BG-UT achieves higher overall classification accuracy and improved recognition of several target sublayers.

The representative well-scale example in Fig. 11 provides a more intuitive illustration of these differences. For well A147, BG-UT shows the closest visual agreement with the expert-interpreted layer sequence and its top and base depths. By comparison, SegNet generates more fragmented intervals near layer transitions, while Encoder Transformer still shows minor boundary oscillations and local misassignments. BG-UT preserves the expected vertical order of 74 to 79 more consistently and produces smoother, more continuous layer segments, which is critical for practical stratigraphic correlation. This example complements the quantitative metrics and reinforces the conclusion that the proposed model is better suited for operational use, where both numerical accuracy and geological plausibility are required.

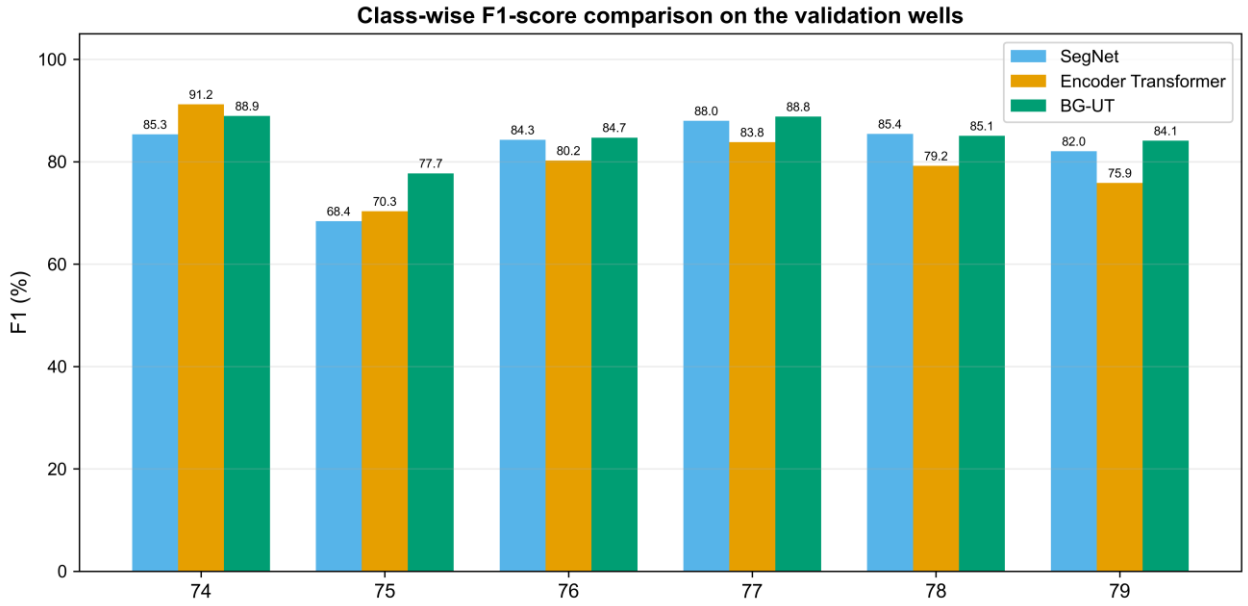


Fig. 10 Class-wise stratigraphic recognition performance of the three models on the validation wells.

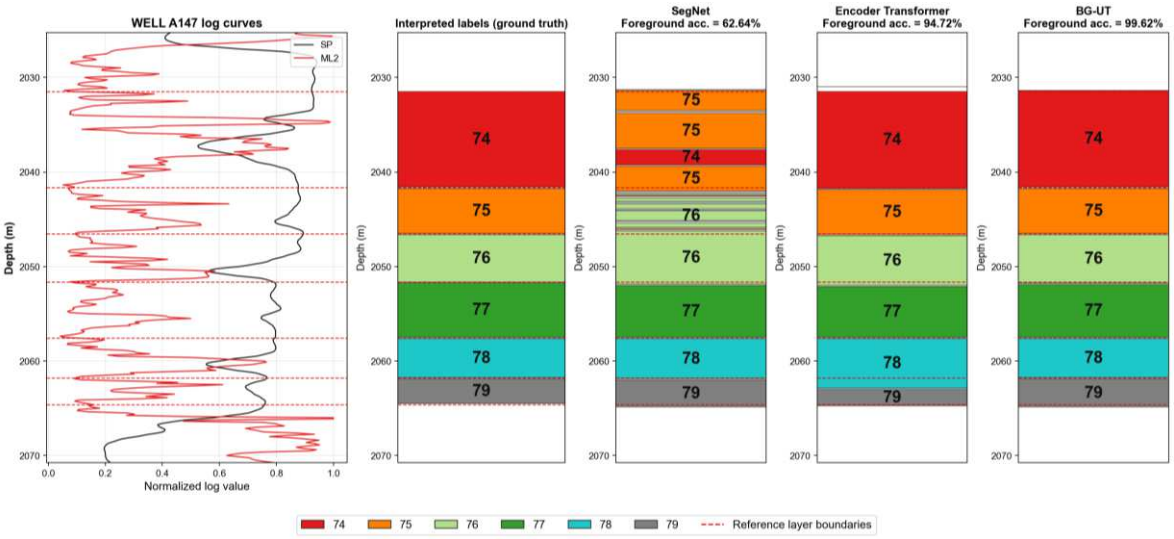


Fig. 11 Representative well-scale comparison between interpreted labels and model predictions.

Effect of sequence-constrained decoding

Sequence-constrained decoding is introduced as a post-processing step to encourage transitions consistent with the prescribed stratigraphic succession and reduce isolated label changes in the point-wise predictions before decoding. Fig. 12 summarizes its impact on the labeled wells. Although the mean accuracy changes only marginally, from 92.25% to 92.30%, the distribution reveals a more nuanced behavior: 66 wells are improved, 166 remain unchanged, and 67 are slightly degraded. The accuracy-change histogram is tightly centered around zero, indicating that the decoder acts conservatively and mainly adjusts predictions near uncertain boundaries rather than rewriting the overall stratigraphic pattern. The scatter plot further suggests that improvements are more evident in wells with moderate accuracy before decoding,

whereas wells that are already highly accurate show little change.

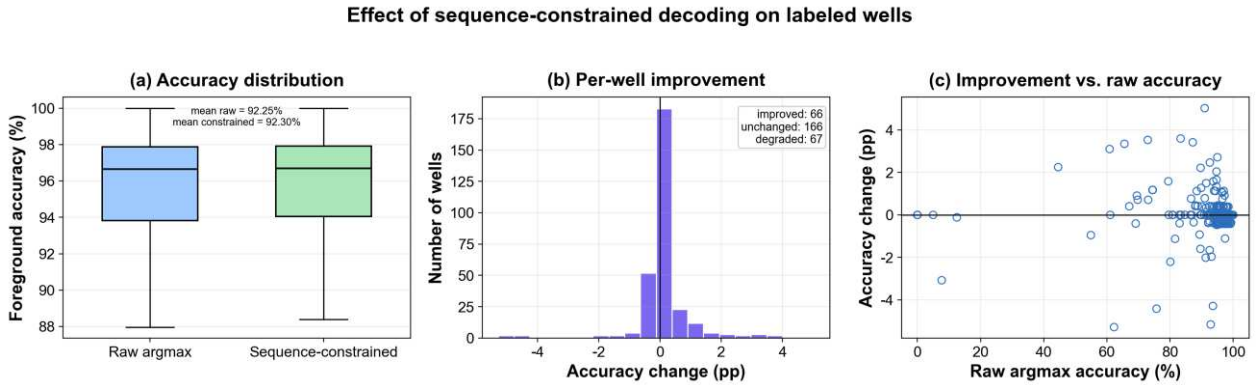


Fig. 12 Paired comparison of BG-UT predictions before and after sequence-constrained decoding across the evaluated labeled wells, including training and validation wells

Fig. 13 provides a representative example. In this well, the point-wise predictions before decoding already capture the main vertical succession, but contain short, isolated label changes near layer boundaries. After sequence-constrained decoding, these local fluctuations are suppressed and the predicted intervals become more geologically coherent, with smoother boundaries and better agreement with the reference stratigraphy. This example illustrates how sequence-constrained decoding reduces local label interruptions and produces more continuous stratigraphic intervals. Across the evaluated wells, its effect on average accuracy remains small.

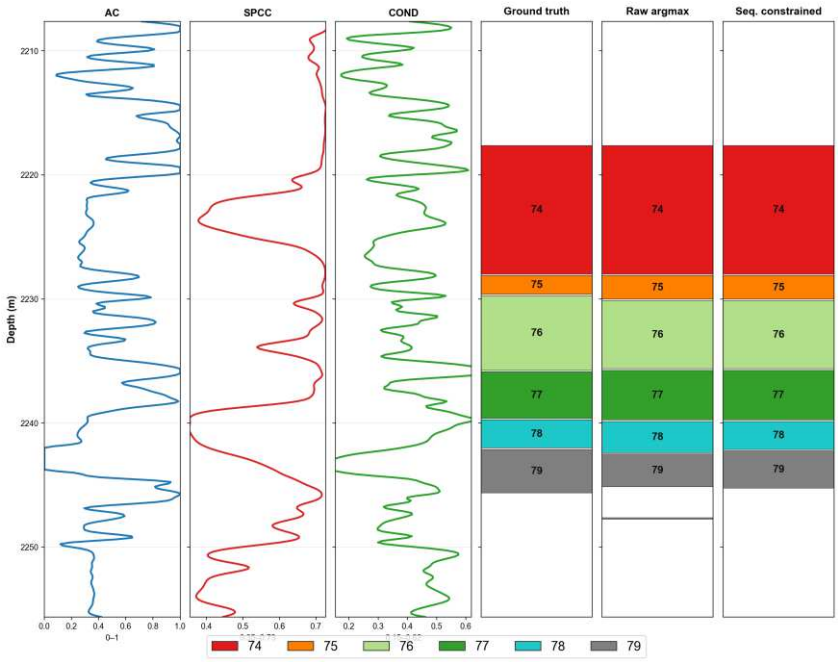


Fig. 13 Representative well-scale stratigraphic correlation example showing the effect of sequence-constrained decoding.

Automatic correlation of unlabeled wells

To examine the continuity of predicted stratigraphic intervals, we visually inspected the results for two representative unlabeled wells. Fig. 14 presents BG-UT automatic correlation results for two representative unlabeled wells, well A371 and well A483. Five well logs, including AC, SPCC, COND, ML1, and ML2, are used as inputs, and the predicted stratigraphic columns are shown on the right. In both wells, BG-UT delineates a coherent shallow-to-deep sequence from sublayer 74 to sublayer 79, with layer boundaries consistent with the major variations in the log responses. Despite differences in log patterns between the two wells, the predicted stratigraphic succession remains continuous and well ordered, indicating good generalization capability on unlabeled wells.

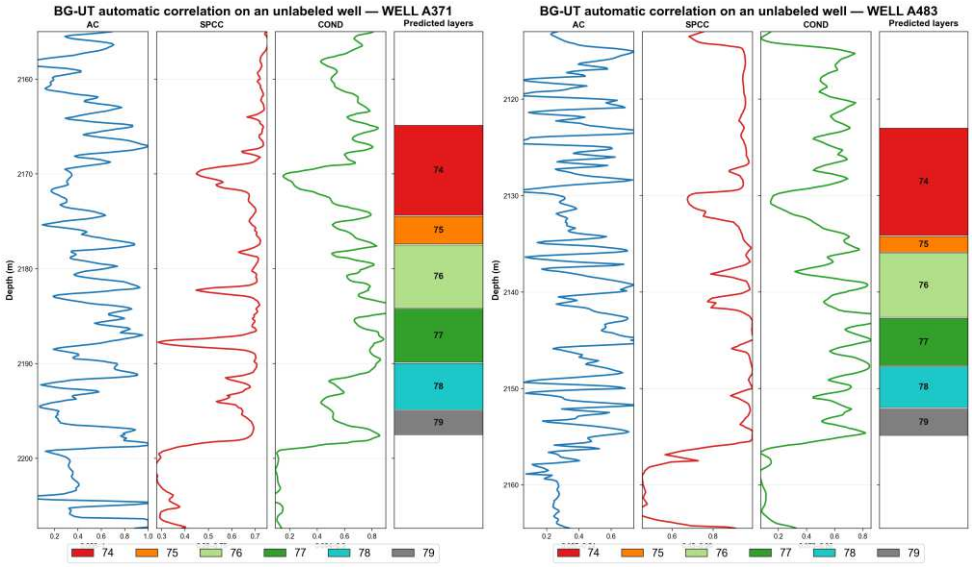


Fig. 14 Representative BG-UT automatic correlation results on unlabeled wells: well A371 and well A483.

To illustrate the application of BG-UT to wells not used in model development, two well-correlation profiles were constructed from the unlabeled wells (Fig. 15). One profile connects seven wells along a southeast–northwest alignment, and the other connects seven wells along a southwest–northeast alignment. These profiles illustrate the application of the trained framework to unlabeled wells along two spatial directions. Fig. 16 presents the corresponding automatic stratigraphic correlation sections generated by BG-UT using the five available logs in each well. The predicted boundaries delineate the target sublayers (74–79) with a consistent vertical order and clear lateral continuity along both profiles. The correlation profiles show visually continuous interfaces between adjacent wells and variations in predicted sublayer thickness. The profiles show slight variations in predicted interface depths and sublayer thickness between adjacent wells. In the NW profile, the sand-prone intervals are more continuous and relatively thicker, whereas the NE profile exhibits slightly weaker continuity and more obvious thinning toward the southeastern side. This contrast suggests that sand bodies are better developed in the northwestern part of the study area than in the southeastern part, consistent with the inferred depositional trend. Overall, the results demonstrate that BG-UT can perform reliable automatic stratigraphic correlation on unlabeled wells and reproduce the main geological architecture of the target interval.

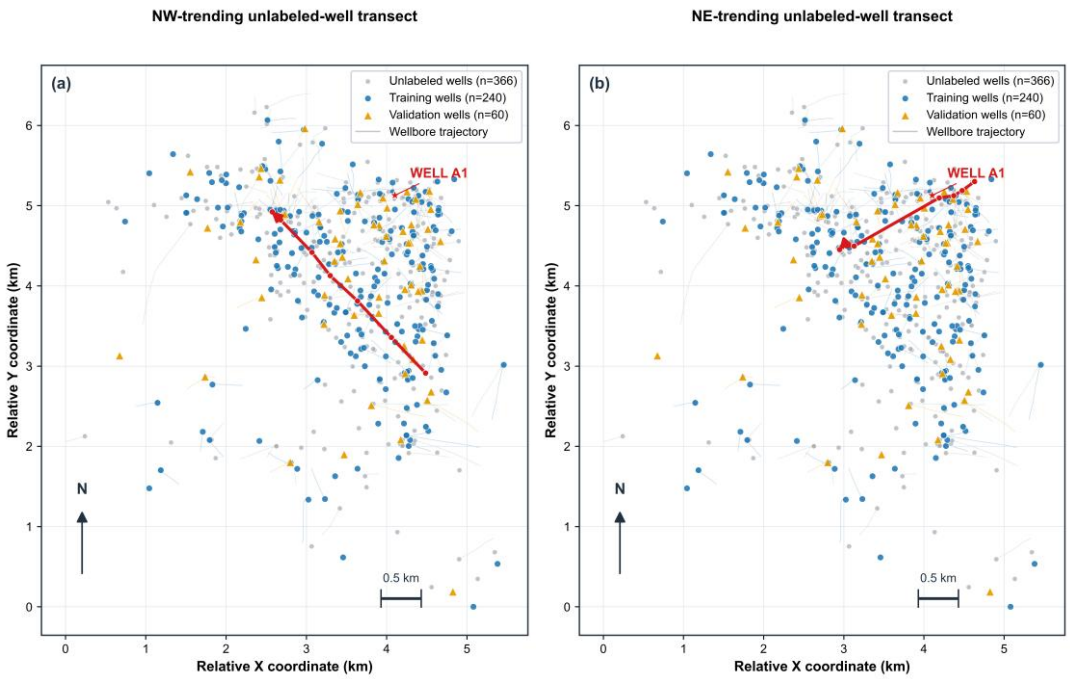


Fig. 15 Spatial distribution of wells and selected NW- and NE-trending unlabeled-well transects

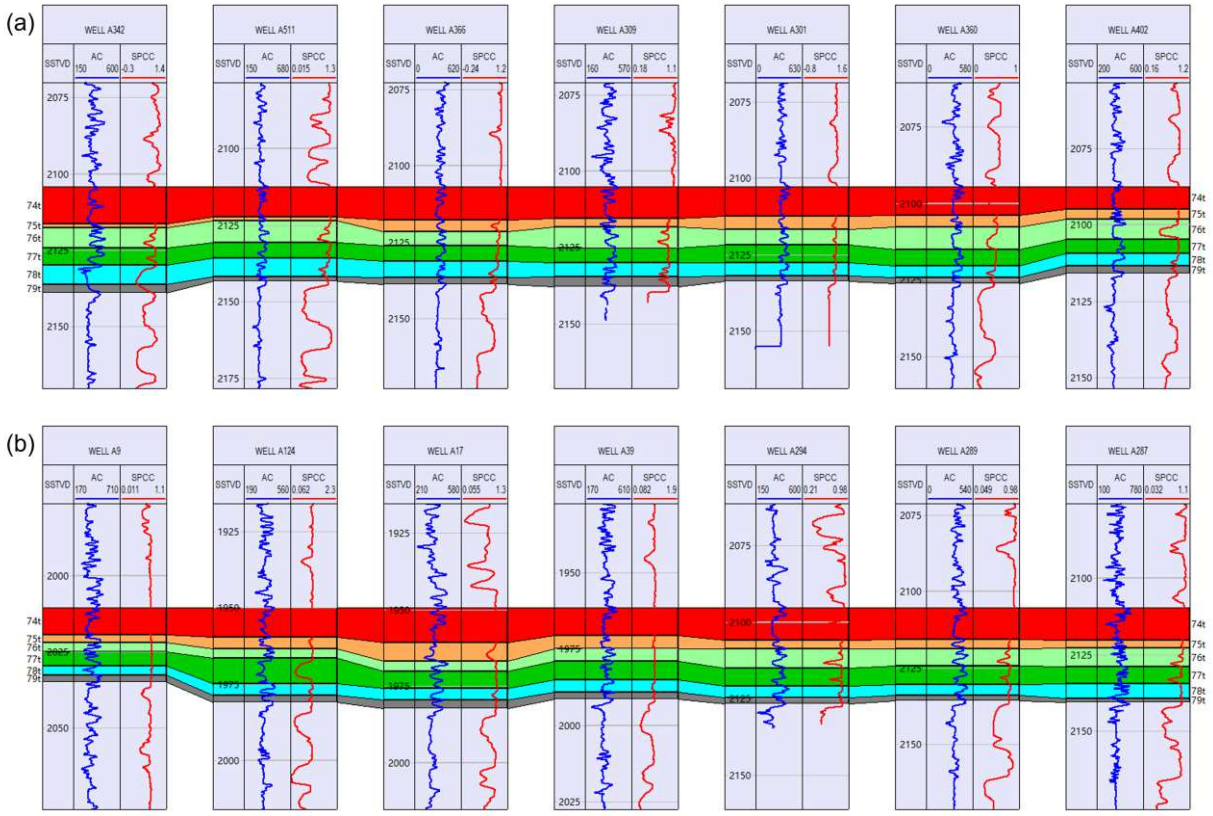


Fig. 16 BG-UT automatic stratigraphic correlation sections along the NW- and NE-trending unlabeled-well transects.

Discussion

Fine-scale stratigraphic correlation requires local response recognition, information from broader depth intervals, and consistency with the expected stratigraphic succession. BG-UT combines convolutional feature extraction and skip connections with a Transformer bottleneck to address these requirements. The convolutional pathway retains local variations, while self-attention relates responses at different depths. Joint top/base-depth regression and boundary detection provide complementary supervision for interval geometry and local class transitions. These auxiliary tasks guide the shared features during training, whereas the exported interfaces are extracted from the refined classification sequence.

The validation results support the effectiveness of the complete framework, with improved aggregate metrics and higher F1-scores for four of the six target sublayers (Table 2 and Fig. 10). The representative well comparison also shows closer agreement with the interpreted intervals (Fig. 11). However, the compared models differ in architecture, supervision, and inference strategy, so the contribution of each component requires further assessment through ablation experiments. Classification metrics should also be complemented by interface-depth errors to evaluate boundary localization directly.

Sequence-constrained decoding produces only a small change in average accuracy, with its main benefit being the adjustment of selected label interruptions and inconsistent transitions (Figs. 12 and 13). Its value therefore lies in improving interval continuity alongside classification performance. The transition model assumes a known vertical succession and requires adjustment where faulting, erosion, missing units, or repeated sections alter that order. Minimum-thickness filtering likewise requires careful calibration because it may merge genuine thin layers as well as prediction fragments.

The framework can be configured for different logging channels and target units, but its performance depends on representative training data and consistent interpretations. Missing curves, changes in measurement conditions, and unfamiliar geological settings may affect predictions. Since the validation set also guides model selection, independent testing and applications in other fields are needed to assess broader generalization.

Conclusions

This study develops a Boundary-Guided U-Transformer framework for automatic stratigraphic correlation from multichannel well logs. The method combines a U-shaped convolutional encoder–decoder with a Transformer bottleneck to integrate local response patterns and information from broader depth intervals. Joint classification, top/base-depth regression, and boundary detection provide complementary supervision for stratigraphic identification and interface-position learning. During inference, a geological transition model and Viterbi decoding incorporate the expected vertical succession, after which predicted labels are converted into contiguous stratigraphic intervals and top/base-depth tables.

On the 60 validation wells, BG-UT achieves an average accuracy of 82.09%, macro precision of 90.18%, macro recall of 80.35%, and macro F1-score of 84.89%. Its average accuracy exceeds that of SegNet and Encoder Transformer by 4.46 and 2.71 percentage points, respectively. BG-UT achieves the highest F1-score for four of the six target sublayers, with a particularly pronounced improvement for sublayer 75.

Sequence-constrained decoding produces only a small change in average classification accuracy but reduces selected local label inconsistencies and improves interval continuity and agreement with the expected succession. Application to 366 unlabeled wells further demonstrates the complete workflow

from multichannel well logs to well-level stratigraphic subdivisions, top/base-depth tables, and multi-well correlation sections.

The framework provides an approach to supporting fine-scale stratigraphic subdivision and correlation in densely drilled reservoirs. Further research could use ablation experiments, interface-depth error analysis, and cross-field validation to clarify the contributions of individual components and refine its application under different geological conditions.

Declarations

Funding: This work was supported by Natural Science Foundation of Sichuan Province (Grant No. 2024NSFSC1992).

Competing interests: The authors declare no competing interests.

Author contributions: Jian Yang: Writing – review & editing, Writing – original draft, Methodology, Formal analysis. Xuri Huang: Writing – review & editing, Supervision, Resources, Funding acquisition. Yumao Chen: Data curation, Resources, Project administration, Writing – review & editing. Jing Tang: Validation. Yuxiao Zhang: Supervision.

Data availability: The authors do not have permission to share data.

References

Badrinarayanan V, Kendall A, Cipolla R (2017) SegNet: A deep convolutional encoder–decoder architecture for image segmentation. IEEE Transactions on Pattern Analysis and Machine Intelligence 39(12):2481–2495. https://doi.org/10.1109/TPAMI.2016.2644615

Behdad A (2019) A step toward the practical stratigraphic automatic correlation of well logs using continuous wavelet transform and dynamic time warping technique. Journal of Applied Geophysics 167:26–32. https://doi.org/10.1016/j.jappgeo.2019.05.007

Caruana R (1997) Multitask learning. Machine Learning 28:41–75. https://doi.org/10.1023/A:1007379606734

Dai Y, Huang X, Liu H, Han Z (2025) A semi-automatic well correlation method for mature oil and gas fields. Journal of Geophysics and Engineering 22(5):1344–1359. https://doi.org/10.1093/jge/gxaf077

Dai Y, Huang X, Liu H, Yang H, Song H (2026) From automated well stratigraphic interpretation to its seismic-constrained spatial mapping using multitask neural network: Implications for reservoir property modeling. Interpretation. https://doi.org/10.1190/INT-2024-0165

Lineman DJ, Mendelson JD, Toksöz MN (1987) Well-to-well log correlation using knowledge-based systems and dynamic depth warping. Technical report, Earth Resources Laboratory, Massachusetts Institute of Technology, Cambridge, MA. https://hdl.handle.net/1721.1/75091

Liu N, Li Z, Chen J, Liu Y, Wu H, Gao J, Zhou X (2022) The edge-guided FPN model for automatic stratigraphic correlation of well logs. Journal of Petroleum Science and Engineering 218:110985. https://doi.org/10.1016/j.petrol.2022.110985

Liu N, Li Z, Liu R, Zhang H, Gao J, Wei T, Si J, Wu H (2023) ASHFormer: Axial and sliding window-based attention with high-resolution transformer for automatic stratigraphic correlation. IEEE Transactions on Geoscience and Remote Sensing 61:1–10. https://doi.org/10.1109/TGRS.2023.3296934

Lu M, Cai D, Fu X, Cheng S, Sun Y, Liu P, Jiao Y (2025) An intelligent log-seismic integrated stratigraphic correlation method based on wavelet frequency-division transform and dynamic time warping: A case study from the Lasaxing oilfield. Energy Geoscience 6(3):100412. https://doi.org/10.1016/j.engeos.2025.100412

Mann CJ, Dowell TPL Jr (1978) Quantitative lithostratigraphic correlation of subsurface sequences. Computers & Geosciences 4(3):295–306. https://doi.org/10.1016/0098-3004(78)90064-X

Raffel C, Shazeer N, Roberts A, Lee K, Narang S, Matena M, Zhou Y, Li W, Liu PJ (2020) Exploring the limits of transfer learning with a unified text-to-text Transformer. Journal of Machine Learning Research 21(140):1–67. https://jmlr.org/papers/v21/20-074.html

Ronneberger O, Fischer P, Brox T (2015) U-Net: Convolutional networks for biomedical image segmentation. In: Medical image computing and computer-assisted intervention—MICCAI 2015. Springer International Publishing, Cham, pp 234–241. https://doi.org/10.1007/978-3-319-24574-4_28

Rudman AJ, Lankston RW (1973) Stratigraphic correlation of well logs by computer techniques. AAPG Bulletin 57(3):577–588. https://doi.org/10.1306/819A4306-16C5-11D7-8645000102C1865D

Sylvester Z (2023) Automated multi-well stratigraphic correlation and model building using relative geologic time. Basin Research 35:1961–1984. https://doi.org/10.1111/bre.12787

Tang L, Li T, Xu C (2024) Stratigraphic division method based on the improved YOLOv8. Applied Sciences 14(20):9485. https://doi.org/10.3390/app14209485

Vaswani A, Shazeer N, Parmar N, Uszkoreit J, Jones L, Gomez AN, Kaiser L, Polosukhin I (2017) Attention is all you need. In: Advances in neural information processing systems 30. Curran Associates, Inc. https://papers.nips.cc/paper/7181-attention-is-all-you-need

Viterbi A (1967) Error bounds for convolutional codes and an asymptotically optimum decoding algorithm. IEEE Transactions on Information Theory 13(2):260–269. https://doi.org/10.1109/TIT.1967.1054010

Wang CZ, Wei XY, Pan HX, Han LF, Wang H, Wang HQ, Zhao H (2024) Well logging stratigraphic correlation algorithm based on semantic segmentation. Applied Geophysics 21(4):650–666. https://doi.org/10.1007/s11770-024-1085-8

Wheeler L, Hale D (2014) Simultaneous correlation of multiple well logs. In: SEG technical program expanded abstracts 2014, pp 618–622. https://doi.org/10.1190/segam2014-0227.1

Xu Z, Zheng B, Liu B, Song W (2025) Stratigraphic correlation of well logs using geology-informed deep learning networks. Processes 13(5):1288. https://doi.org/10.3390/pr13051288

Yang Y, Wang J, Li Z, Liu N, Liu R, Gao J, Wei T (2023) Automated stratigraphic correlation of well logs using attention based dense network. Artificial Intelligence in Geosciences 4:128–136. https://doi.org/10.1016/j.aiig.2023.09.001

Zhang H, Liu N, Wu H, Huo J (2025) Stratigraphic sequence correlation of well logs using KANFormer enhanced with OMP-based data augmentation. IEEE Transactions on Geoscience and Remote Sensing 63:1–11. https://doi.org/10.1109/TGRS.2025.3532442